International Journal of Minerals, Metallurgy and Materials
Volume 20, Number 7, July 2013, Page 684
DOI: 10.1007/s12613-013-0784-6

Numerical simulation of temperature field in horizontal core-filling continuous casting for copper cladding aluminum rods

Ya-jun Su, Xin-hua Liu, Yong-fu Wu, Hai-you Huang, and Jian-xin Xie

Key Laboratory for Advanced Materials Processing (Ministry of Education), Institute of Advanced Materials and Technology, University of Science and Technology Beijing, Beijing 100083, China

(Received: 13 April 2012; revised: 27 February 2013; accepted: 28 February 2013)

Abstract: The steady-state temperature field of horizontal core-filling continuous casting (HCFC) for producing copper cladding aluminum rods was simulated by finite element method to investigate the effects of key processing parameters on the positions of solid-liquid interfaces (SLIs) of copper and aluminum. It is found that mandrel tube length and mean withdrawing speed have significant effects on the SLI positions of both copper and aluminum. Aluminum casting temperature (T_{Al}) (1003-1123 K) and secondary cooling water flux (600-900 $L \cdot h^{-1}$) have little effect on the SLI of copper but cause the SLI of aluminum to move 2-4 mm. When T_{Al} is in a range of 1043-1123 K, the liquid aluminum can fill continuously into the pre-solidified copper tube. Based on the numerical simulation, reasonable processing parameters were determined.

Keywords: metal cladding; copper; aluminum; continuous casting; interfaces; computer simulation

1. Introduction

Since 1960s, many technologies for fabricating copper cladding aluminum (CCA) bimetal conductors have been developed, for instance, continuous electroplating [1], co-rolling [2], overlay welding [3], and hydrostatic extrusion [4]. However, these technologies have some common shortages, such as long process and difficulty in producing CCA composite conductors with a large or complicated-shaped cross section.

Horizontal core-filling continuous casting (HCFC) [5-8] is a novel technology for fabricating bimetal composite materials, which has some advantages, such as short process, low production cost, metallurgical bonding interfaces, and suitable for manufacturing large and complicated-shaped cross section products. In addition, since the continuous casting direction is parallel to the ground, HCFC also has advantages of easy operation and convenience for continuous production.

A key problem for fabricating CCA rods by HCFC technology is how to optimize processing parameters to ensure a well filling of liquid aluminum into pre-solidified copper tubes and avoid excess interface reaction between liquid aluminum and solid copper, which finally control the quality of products.

The HCFC process is mainly controlled by five processing parameters: temperatures of liquid copper and aluminum, primary cooling intensity, secondary cooling intensity, and casting speed. Numerical simulation is an effective method to analyze coupling multifactor problems with complex boundary conditions [9-11].

In this work, CCA rods with a diameter of 30 mm were selected as a research object, and the effects of processing parameters on the temperature field of HCFC for CCA rods were numerically simulated by finite element method (FEM) using ProCAST software in order to provide a theoretical reference for optimizing the HCFC process.

2. Model and simulation method

2.1. HCFC process

The schematic diagram of HCFC is shown in Fig. 1. The principle of HCFC for producing CCA rods could be described as follows. First, liquid copper in crucible 5 was cast into the compound mold in crystallizer 7 continuously and solidified into a copper tube. Then, liquid aluminum in

Corresponding author: Xin-hua Liu E-mail: Liuxinhua18@163.com

crucible 1 was injected into the pre-solidified copper tube continuously through mandrel tube 11 and solidified into aluminum core cooled by composite crystallizer 7 and secondary cooling water 8. Thus, a CCA rod with a metallurgical bonding interface was fabricated.

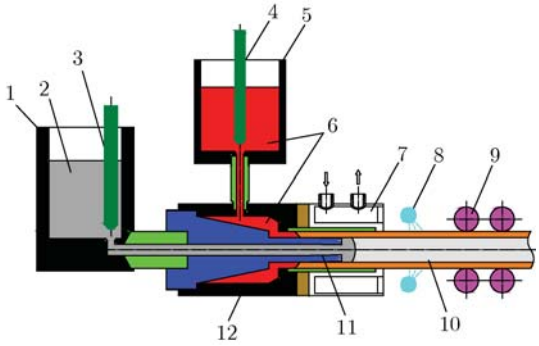

Fig. 1. Schematic diagram of HCFC for copper cladding aluminium: 1 — crucible for aluminium; 2 — molten aluminium; 3, 4 — stopper; 5 — crucible for copper; 6 — molten copper; 7 — crystallizer for composite continuous casting; 8 — secondary cooling water; 9 — withdrawing mechanism; 10 — CCA composite rod; 11 — mandrel tube; 12 — insulating chamber.

2.2. Heat transfer equation and temperature field model

The temperature field during casting is calculated based on the heat conduction differential equation of energy conservation [12]:

$$\rho C_p \left(\frac{\partial T}{\partial t}\right) = \lambda \left(\frac{\partial^2 T}{\partial x^2} + \frac{\partial^2 T}{\partial y^2} + \frac{\partial^2 T}{\partial z^2}\right) + L_s \frac{\partial f_s}{\partial t} \qquad (1)$$

where ρ is the density, kg·m^{-3}; C_p is the specific heat capacity, J·kg^{-1}·K^{-1}; λ is the thermal conductivity, W·m^{-1}·K^{-1}; T is the temperature, K; t is the time, s; x, y, and z are spatial coordinate axes, mm; L_s is the latent heat of solidification, J·kg^{-1}; and f_s is the solid phase fraction in the solidification.

During HCFC process, the CCA rod was solidified in the molds. Based on physical principle of HCFC, a 2D axial symmetry model was established due to the axial symmetry geometry of the billet and casting molds, as shown in Fig. 2. The model consists of the copper tube, aluminum core, graphite mold, graphite mandrel tube, and water cooling copper sleeve.

The 2D axial symmetry model was built using ProCAST software. The copper tube was divided into 1 mm × 0.25 mm rectangular meshes, the aluminum core was divided into triangular meshes with the side length of 1 mm, and the rest was set as triangle meshes with the maximum side length of 2 mm. The automatically generated meshes had good convergence with the other different meshes.

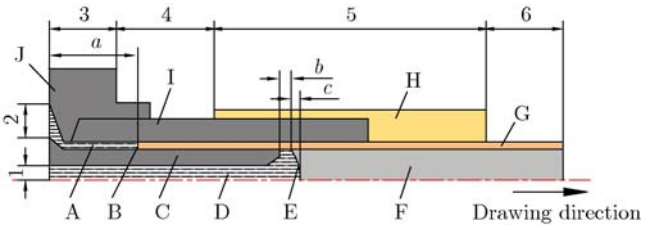

Fig. 2. Geometric model of horizontal core-filling continuous casting: A — liquid copper; B — solid-liquid interface of copper; C — mandrel tube; D — liquid aluminum; E — solid-liquid interface of aluminum; F — solidified aluminum core; G — copper sheath; H — water cooling copper sleeve; I — graphite casting mold; J — insulating chamber; 1-6: boundary of heat transfer; *a-c*: position parameters of solid-liquid interfaces of copper and aluminum, *a* — distance from the copper solid-liquid interface to the left side of the mandrel, *b* — distance from the aluminum solid-liquid interface to the outlet of the mandrel, *c* — liquid pool depth of aluminum.

2.3. Basic assumptions and boundary conditions

As mentioned above, the process of HCFC mainly includes two parts. First, the copper tube is cast continuously. Second, the molten aluminum fills into the pre-solidified copper tube, which acts as a casting mold and is solidified under the cooling of primary and secondary cooling water. Therefore, the whole temperature field simulation could be performed by two steps. The first step is to obtain the casting temperature field of the copper tube. The second step is to obtain the composite continuous casting temperature field of the CCA rod. The steady state temperature field of the copper tube obtained by the first step was loaded as the initial condition into the second step.

During the simulation, the HCFC process can be simplified as follows.

(1) Simulation is conducted based on steady-state processing, and only the stable temperature field is considered at the setting boundary conditions.

(2) The convection heat transfer and natural convection inside the molten metals are ignored.

(3) All the components keep isotropic, and their physical parameters are only related to temperature.

(4) Only the latent heat of solidification is considered, and heat of other phase transformation is ignored.

(5) Primary cooling water and secondary cooling water distribute uniformly along the billet circumference and the cooling intensity is also uniform along the circumference.

The heat transfer boundary conditions for the analysis of temperature field are set as follows.

Boundary 1, 2: boundary of constant temperature.

The casting temperatures of copper and aluminum are set as the first boundary condition.

Boundary 3: boundary of the insulating chamber. External heating under the experimental conditions, the surface heat radiation coefficient and the outside temperature are set according to the third boundary condition.

Boundary 4: contact boundary of the crystallizer. The furnace wall and the insulation material are set as the adiabatic boundary.

Boundary 5: boundary of primary water cooling. The temperature of cooling water and the heat transfer coefficient are set according to the third boundary condition.

Boundary 6: air cooling region and cooling region of secondary cooling water. The heat exchange coefficient and the temperatures of air and cooling water are set according to the third boundary condition.

The rest boundaries are set as the adiabatic boundary condition.

2.4. Material data and heat transfer coefficient

2.4.1. Material data

During the numerical simulation of temperature field of HCFC, the materials included copper, aluminum, and graphite. The variation of material parameters with temperature has effect on the simulation results. Considering the accuracy of the results, the variation should be considered. In the experiment, the cladding layer was made of 99.5wt% pure copper, the aluminum core was 99.7wt% pure aluminum, and the casting molds were made of "3H" (high density, high strength, and high purity) graphite. According to actual measurement, the density of "3H" graphite is about 1900 $kg{\cdot}m^{-3}$ (slightly less than the theoretical density of 2200 $kg{\cdot}m^{-3}$), and the specific heat is set as a constant value of 750 $J{\cdot}kg^{-1}{\cdot}K^{-1}$. The variation of physical parameters of the three materials with temperature can be obtained from relevant references [13-15].

2.4.2. Calculation of heat transfer coefficient

(1) Convection heat transfer coefficient of primary cooling water.

Primary cooling water in the crystallizer flows along a horizontal annular gap. The interfacial heat transfer coefficient between the primary cooling water and the copper sleeve can be calculated according to convection heat transfer of the annular space liquid. For different section shapes of pipes, feature size should be first defined for calculation of Reynolds number (Re) and Nusselt number (Nu) [16]. The feature size of the pipe can be used as an equivalent diameter (d_e) in hydromechanics, which is defined as

$$d_e = \frac{4A}{P} \tag{2}$$

where A is the cross-sectional area of the pipe and P is the wet perimeter, namely the contact length between the fluid and the cross section.

For a circular pipe, the fluid flows between two concentric tubes, and the equivalent diameter can be written as

$$d_e = \frac{4\pi\left[(D/2)^2 - (d/2)^2\right]}{\pi(D+d)} = D - d \tag{3}$$

where D is the external diameter and d is the internal diameter. Thus, the heat transfer coefficient of cooling water can be calculated as

$$h_1 = \frac{Nu_f \cdot \lambda_f}{d_e} \tag{4}$$

where λ_f is the thermal conductivity of water, and Nu_f is the Nusselt number of flow, which can be calculated according to Refs. [12-13].

(2) Convection heat transfer coefficient of secondary cooling water.

Water spray cooling method is used in the secondary cooling of HCFC. Cooling water is injected directly on the billet surface. The boundary of secondary water cooling refers to the study proposed by Weckman and Niessen [17], where the boundary condition of the spray cooling regions is considered as the combination of the forced convective and boiling heat transfer.

When the billet surface temperature is relatively low, the forced convection heat transfer coefficient between the billet surface and the washing water can be calculated as follows:

$$h_{c2} = \left(-1.67 \times 10^5 + 704\bar{T}\right) Q'^{1/3} \tag{5}$$

where $\bar{T} = (T_{sur} + T_w)/2$ is the average water temperature, T_{sur} is the billet surface temperature, and T_w is the temperature of cooling water, K. The thermophysical material properties of water must be evaluated at the average temperature. $Q' = Q/(\pi D_b)$ is the volume flow rate of cooling water per unit circumference, $m^2{\cdot}s^{-1}$; Q is the total cooling water flux, $m^3{\cdot}s^{-1}$; and D_b is the billet diameter, m.

When the billet surface temperature is higher than the boiling temperature of water, the boiling heat transfer occurs. The boiling heat transfer coefficient between the cooling water and the copper tube surface can be determined by [18-19]

$$h_{b2} = (-1.67 \times 10^5 + 704\bar{T})Q'^{1/3} + \frac{30.8}{\Delta T_2}(\Delta T_x)^3 \tag{6}$$

where $\Delta T_2 = T_{sur} - T_w$ is the temperature difference between the billet surface and the cooling water; $\Delta T_x = T_{sur} - T_{sat}$, and T_{sat} is the saturation temperature of water, K.

(3) The heat transfer coefficient between the billet surface and air.

When the billet is pulled out of the crystallizer, radiation heat transfer and free convective heat transfer between the billet and the surrounding air occurs. Therefore, the heat transfer boundary conditions can be written as

$$h_3 = h_{c3} + h_{r3} \tag{7}$$

where h_{c3} is the free convection heat transfer coefficient, W·m·K^{-1}; h_{r3} is the radiation heat transfer coefficient, W·m·K^{-1}.

Assuming the air temperature as a constant of 298 K (25°), the free convection heat transfer coefficient of billets with different surface temperatures can be calculated as [12]

$$h_{c3} = \frac{\left\{0.60 + \frac{0.387Ra^{1/6}}{[1+(0.559/Pr)^{9/16}]^{8/27}}\right\} \cdot \lambda_a}{l_c} \quad (8)$$

where $Ra = Gr \cdot Pr$ is the Rayleigh number, λ_a is the thermal conductivity between air and the solidified billet surface, $Gr = \frac{g \cdot \alpha_V \cdot \Delta T_3 \cdot l_c^3}{\nu^2}$ is the Grashof number, Pr is the Prandtl number, g is the acceleration of gravity, m·s^{-2}; α_V is the gas volume expansion coefficient, K^{-1}; $\Delta T_3 = T_{sur} - T_{amb}$ is the difference between the surface temperature (T_{sur}, K) and ambient air temperature (T_{amb}, K), K; l_c is the feature size of the billet, m; and ν is the movement viscosity of air, m^2·s^{-1}.

The radiation heat transfer coefficient between the billet surface and air can be determined by

$$h_{r3} = \frac{\varepsilon \cdot c_b \cdot \left[\left(\frac{T_{sur}}{100}\right)^4 - \left(\frac{T_\infty}{100}\right)^4\right]}{T_{sur} - T_\infty} \quad (9)$$

where ε is the emissivity of the body; c_b is the radiation coefficient of the black body, W·m^{-2}·K^{-4}; T_{sur} is the surface temperature of the body, K; and T_∞ is the temperature in infinite distance, K.

2.5. Verification of the model

Before continuous casting, holes with different depths into the graphite casting mold (Fig. 2, I) were drilled from the outlet of the crystallizer and then K-type thermocouples with the diameter of 0.5 mm were put into the holes. The temperature field calculated by the FEM model was evaluated by comparing the simulated temperature and the measured value at the same point. The simulated temperature field and the positions of the drilled points are shown in Fig. 3, where T_0 was the deepest temperature measuring point in the crystallizer graphite mold, and two adjacent measuring points had an interval of 10 mm.

The measured and the simulated temperatures of T_0-T_8 are shown in Table 1. It can be seen that the deviation between the simulated temperature and measured temperature is less than 10%, which indicates that the above model can meet the precision of engineering calculation.

2.6. Simulation conditions

The cross-section size of the casting billet for simulation is 30 mm in diameter and 3 mm in the thickness of the copper cladding layer. Specific simulation conditions are shown in Table 2.

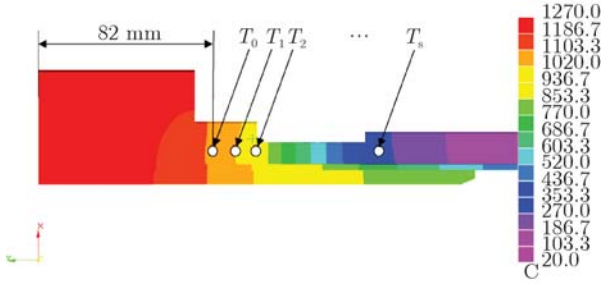

Fig. 3. Temperature measurement points of HCFC for fabricating CCA rods.

Table 1. Comparison between the measured and simulated temperature of HCFC for fabricating CCA rods

Measurement point	Measured values / K	Average value / K	Simulated value / K	Deviation / %
T_0	1350, 1343, 1348	1347	1364	1.6
T_1	1285, 1279, 1282	1282	1309	2.7
T_2	1208, 1174, 1160	1181	1230	5.4
T_3	1141, 1089, 1082	1104	1103	–0.1
T_4	1053, 992, 983	1009	974	–4.8
T_5	903, 879, 873	885	857	–4.6
T_6	797, 773, 783	784	749	–6.8
T_7	694, 672, 673	680	645	–8.6
T_8	599, 581, 584	588	574	–4.4

Table 2. Processing parameters for simulation

Processing parameters	Values
Copper casting temperature, T_{Cu} / K	1503
Length of crystallizer / mm	140
Length of mandrel tube, L / mm	190, 210, 230
Aluminum casting temperature, T_{Al} / K	1003, 1043, 1063, 1083, 1103, 1123
Withdrawing speed, v / (mm·min^{-1})	60, 75, 100
Flux of primary cooling water, Q_1 / (L·h^{-1})	450, 600
Flux of second cooling water, Q_2 / (L·h^{-1})	600, 700, 800, 900

In order to investigate the effects of various parameters on the temperature field, both the steady state temperature field and positions of solid-liquid interfaces during HCFC were simulated on the condition that only one processing parameter changed and the other processing parameters remained unchanged. Finally, optimized simulation of the processing parameters was conducted according to the simulation results.

3. Simulation results, analysis, and experiments

3.1. Effect of the mandrel tube length

Fig. 4 and Table 3 show the effects of L on the solid-liquid interface (SLI) positions of copper and aluminum, respectively, under the condition of T_{Cu} = 1503 K, T_{Al} = 1003 K, $Q_1 = Q_2$ = 600 L·h^{-1}, and v = 60 mm·min^{-1}.

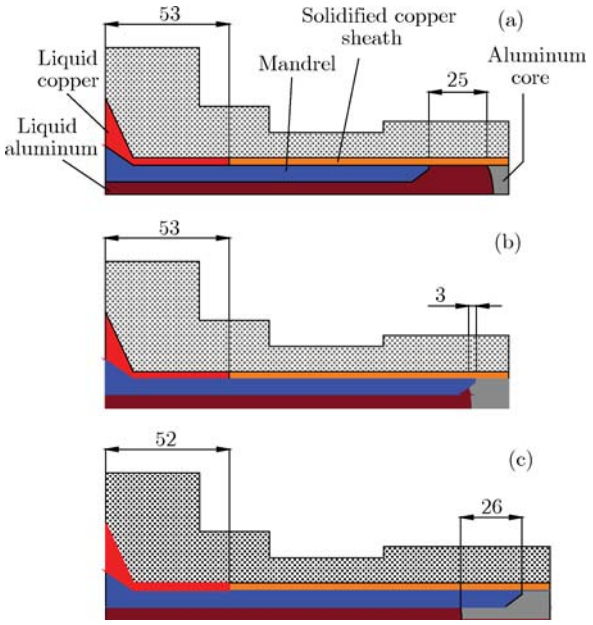

Fig. 4. SLI positions of copper and aluminum in the casting mold when casting CCA rods at different mandrel lengths: (a) L = 190 mm; (b) L = 210 mm; (c) L = 230 mm.

Table 3. Relationship between the mandrel length and the SLI positions of copper and aluminum

L / mm	a / mm	$\|b\|$ / mm	c / mm
190	53	25	4
210	53	3	0
230	52	26	0

Notes: a, b, and c with reference to Fig. 2. Other processing parameters are as follows: T_{Cu} = 1503 K, T_{Al} = 1003 K, $Q_1 = Q_2$ = 600 L·h^{-1}, and v = 60 mm·min^{-1}.

In Fig. 4 and Table 3, the mandrel tube length L has a great influence on the SLI position of aluminum but little influence on that of copper. When L increases from 190 to 230 mm, the distance between the SLI front of aluminum and the outlet of the mandrel tube varies from 25 mm outside of the mandrel tube (Fig. 4(a)) to 26 mm inside of the mandrel tube (Fig. 4(c)), while the SLI position of copper varies only 1 mm against the withdrawal direction.

In Fig. 4 and Table 3, it can also be inferred that the mandrel tube length determine whether liquid aluminum can fill continuously into the tubular copper sheath via the mandrel tube because if the mandrel tube length is too long, the SLI front of aluminum is easy to locate in the mandrel tube and liquid aluminum is plugged in it. At the same time, the interface reaction extent between liquid aluminum and the inner surface of the tubular copper sheath also depends on the mandrel tube length. The reaction extent is greatly influenced by the factors, such as the contact temperature (T_C), length (L_C) and time (t_C) between liquid aluminum and solid copper and the cooling rate (V_{CR}) of CCA rods. Apparently, liquid aluminum can fill continuously into the tubular copper sheath via the mandrel tube if L is in an appropriate range (190 mm $\leq L \leq$ 210 mm). However, the shorter the mandrel tube is, the higher the T_C is, the longer both the L_C and t_C are, or the slower V_{CR} is, thus the severer the interface reaction is. If the mandrel tube is too short, an excessive interface reaction between liquid aluminum and the pre-solidified copper tube will occur due to a very high T_C and long L_C or t_C. Therefore, the optimal mandrel tube length is approximately 210 mm on the basis of the simulated results presented in Fig. 4 and Table 3.

3.2. Effect of aluminum casting temperature

Fig. 5 and Table 4 illustrate the effects of T_{Al} on the SLI positions of copper and aluminum, respectively, under the condition of L = 210 mm, T_{Cu} = 1503 K, $Q_1 = Q_2$ = 600 L·h^{-1}, and v = 60 mm·min^{-1}. The results show that

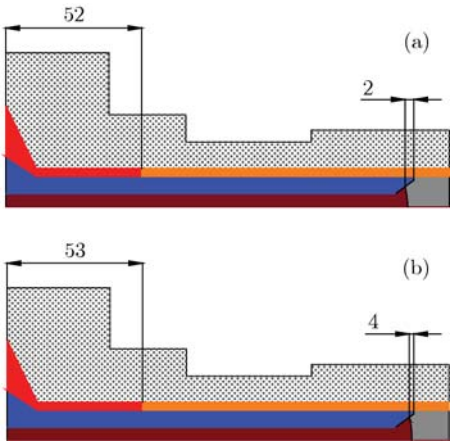

Fig. 5. SLI positions of copper and aluminum in the composite mold when casting CCA rods at different casting temperatures of aluminum: (a) T_{Al} = 1003 K and (b) T_{Al} = 1123 K.

Table 4. Relationship between aluminum casting temperature and the SLI positions of copper and aluminum

T_{Al} / K	a / mm	$\|b\|$ / mm	c / mm
1003	52	4	0
1043	53	3	0
1123	53	2	0

Notes: a, b, and c with reference to Fig. 2. Other processing parameters are as follows: L = 210 mm, T_{Cu} = 1503 K, $Q_1 = Q_2$ = 600 L·h^{-1}, and v = 60 mm·min^{-1}.

when T_{Al} increases from 1003 to 1123 K, the SLI position of aluminum varies from a distance of 4 mm away from the mandrel tube outlet (Fig. 5(a)) to that of 2 mm (Fig. 5(b)), while the SLI position of copper varies only 1 mm along the withdrawal direction of the CCA rod.

3.3. Effect of secondary cooling water flux

Fig. 6 and Table 5 show the effect of the Q_2 on the SLI positions of copper and aluminum, respectively, under the condition of L = 210 mm, T_{Cu}=1503 K (1230°C), T_{Al} =1063 K (790°C), Q_1 =600 L·h^{-1}, and v = 60 mm·min^{-1}.

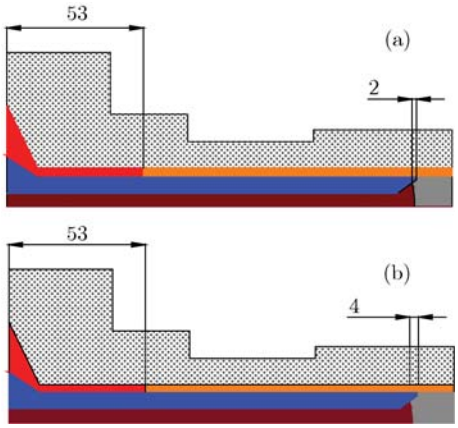

Fig. 6. SLI positions of copper and aluminum in the composite mold when casting CCA rods at different secondary cooling water fluxes: (a) Q_2 = 600 L·h^{-1} and (b) Q_2 = 900 L·h^{-1}.

Table 5. Relationship between the secondary cooling water flux and the SLI positions of copper or aluminum

Q_2 / (L·h^{-1})	a / mm	$\|b\|$ / mm	c / mm
600	53	2	0
700	53	3	0
900	53	4	0

Notes: a, b, and c with reference to Fig. 2. Other processing parameters are as follows: L = 210 mm, T_{Al} = 1063 K, T_{Cu} = 1503 K, Q_1 = 600 L·h^{-1}, and v = 60 mm·min^{-1}.

When Q_2 increases from 600 L·h^{-1} (Fig. 6(a)) to 900 L·h^{-1} (Fig. 6(b)), the SLI position of aluminum moves 2 mm in the opposite direction along withdrawing movement of CCA rods, while the SLI position of copper remains almost unchanged due to the larger distance between the SLI position of copper and the secondary cooling zone.

3.4. Effect of the mean withdrawing speed

Fig. 7 and Table 6 show the effect of mean withdrawing speed on the SLI positions of copper and aluminum under the conditions of L = 210 mm, T_{Cu} = 1503 K, T_{Al} = 1063 K, Q_1 = 600 L·h^{-1}, and Q_2 = 900 L·h^{-1}. Fig. 8 illustrates the relationship between the interface temperature of CCA rods and the distance from the mandrel outlet to the measurement points at the interface.

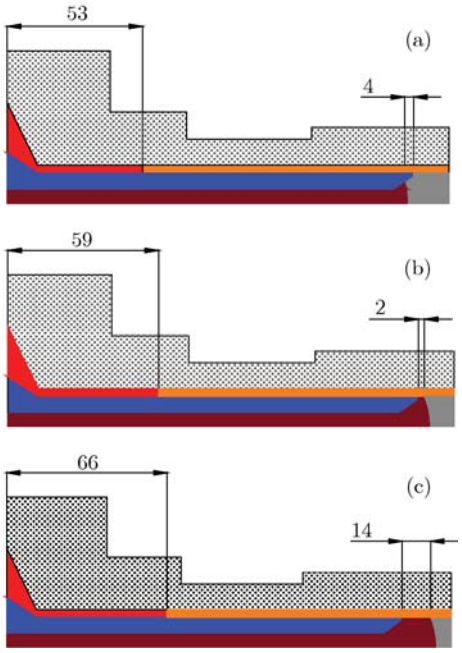

Fig. 7. SLI positions of copper and aluminum in the composite mold when casting CCA rods at different mean withdrawing speeds: (a) v = 60 mm·min^{-1}; (b) v = 75 mm·min^{-1}; (c) v = 100 mm·min^{-1}.

Table 6. Relationship between the mean withdrawing speed and the SLI positions of copper or aluminum

v / (mm·min^{-1})	a / mm	$\|b\|$ / mm	c / mm
60	53	4	0
75	59	2	3
100	66	14	6

Notes: a, b, and c with reference to Fig. 2. Other processing parameters are as follows: L = 210 mm, T_{Cu} = 1503 K, T_{Al} = 1063 K, Q_1 = 600 L·h^{-1}, and Q_2 = 900 L·h^{-1}.

When v increases from 60 to 100 mm·min^{-1}, the SLIs of both copper and aluminum remarkably vary along the withdrawal direction of CCA rods, and the interface temperature between the copper sheath and aluminum core also increases. Fig. 7 and Table 6 also indicate that the SLI position of aluminum lies out of the mandrel tube when

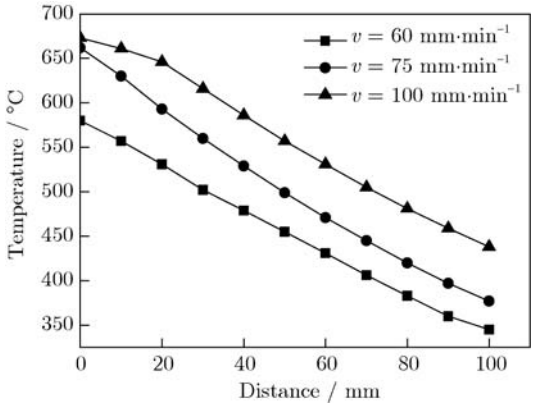

Fig. 8. Relationship between the interface temperature and the distance from the outlet to the measurement points at the interface.

the mean withdrawing speed exceeds 75 mm·min^{-1}, which facilitates to ensure the continuity of core-filling of liquid aluminum.

3.5. Optimization of processing parameters

Based on above analyses, the processing parameters of HCFC for CCA rods are optimized. All the optimized parameters that are used for the numerical simulation of the temperature field are tabulated in Table 7. The relationship between the parameters and the SLI positions of copper and aluminum is shown in Table 8.

From Table 7 and Table 8, it can be seen that the withdrawing speed v, as the key processing parameter, has a remarkable effect on the SLI positions of copper and aluminum.

The appropriate processing parameters of HCFC for producing CCA rods can be listed as follows: v = 75-80 mm·min^{-1}, T_{Cu} = 1503 K, T_{Al} = 1043-1083 K, Q_1 = 600 L·h^{-1}, and Q_2 = 600-900 L·h^{-1}.

Table 7. Processing parameters for optimizing simulation

No.	T_{Cu} / K	T_{Al} / K	Q_1 / (L·h^{-1})	Q_2 / (L·h^{-1})	v / (mm·min^{-1})
1	1503	1043	600	600	75
2	1503	1063	600	700	75
3	1503	1083	600	800	75
4	1503	1043	600	700	80
5	1503	1063	600	800	80
6	1503	1083	600	900	80
7	1503	1043	600	900	85
8	1503	1063	600	900	85
9	1503	1083	600	900	85

Table 8. SLI positions of copper and aluminum under the optimized processing parameters

No.	Solid-liquid interface position / mm	
	a	b
1-3	59	2
4-6	62	6
7-9	63	10

3.6. Experiments

Referred to the above results of numeral simulation, two groups of confirmatory experiments were conducted.

Fig. 9 illustrates the longitudinal section morphologies of CCA rods fabricated by HCFC with different values of L and other processing parameters given as follows: T_{Cu} = 1503 K, T_{Al} = 1003 K, $Q_1 = Q_2$ = 600 L·h^{-1}, and v = 60 mm·min^{-1}.

When L is 190 mm, there is no distinct hollow but some cracks in the aluminum core and the sheath thickness are not uniform because the upper copper sheath of the rod is corroded seriously. When L increases to 210 mm, the sheath thickness is uniform in the industry tolerance range, but there is some distinct shrinkages in the core. When L further increases to 230 mm, there are many hollows or shrinkages in the aluminum core because of the discontinuity of core filling of liquid aluminum during HCFC for the CCA rod.

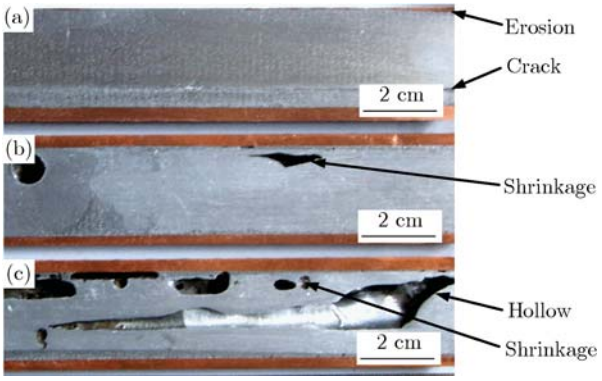

Fig. 9. Longitudinal section morphologies of CCA rods fabricated using different mandrel lengths: (a) L = 190 mm; (b) L = 210 mm; (c) L = 230 mm. T_{Cu} = 1503 K, T_{Al} = 1003 K, and $Q_1 = Q_2$ = 600 L·h^{-1}, and v = 60 mm·min^{-1}.

Fig. 10 shows the longitudinal section morphologies of CCA rods fabricated by HCFC with different values of v and other processing parameters given as follows: L = 210 mm, T_{Cu} = 1503 K, T_{Al} = 1003 K, Q_1 = 600 L·h^{-1} ,

and Q_2 = 900 L·h^{-1}. It can be seen that when v is 60 mm·min^{-1}, some shrinkages exist in the aluminum core because of the discontinuity of core-filling of liquid aluminum during HCFC for the CCA rod. When v further increases to 75 mm·min^{-1}, no distinct shrinkage and cold shut are observed in the core, and the sheath thickness is uniform, which meets the industry requirement. When v further increases to 100 mm·min^{-1}, there are no distinct shrinkage or cold shut in the core, but the upper copper sheath of the rod is corroded.

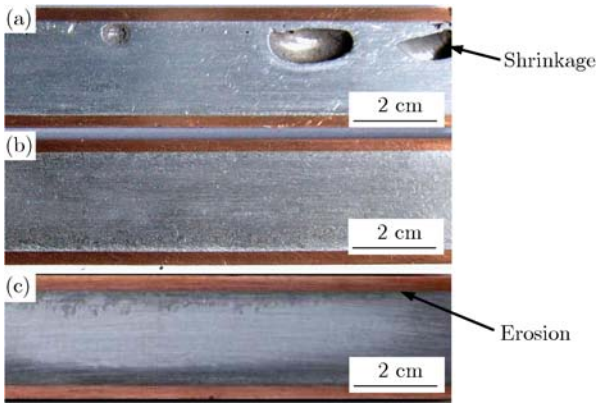

Fig. 10. Longitudinal section morphologies of CCA rods fabricated at different mean withdrawing speeds: (a) v = 60 mm·min^{-1}; (b) v = 75 mm×min^{-1}; (c) v = 100 mm·min^{-1}. L = 210 mm, T_{Cu} = 1503 K, T_{Al} = 1063 K, Q_1 = 600 L·h^{-1}; Q_2 = 900 L·h^{-1}.

All the above experimental results are in good agreement with the corresponding numerical simulation results (Fig. 4 and Fig. 7) and analyses.

4. Conclusions

(1) The optimal length of mandrel tube is approximately 210 mm. If the mandrel tube is too short (e.g., L = 190 mm), the SLI position of aluminum is located far away from the mandrel tube outlet, which results in the formation of interface erosion defects in CCA rods. Conversely, the SLI position of aluminum is located into the mandrel tube, which induces the discontinuity of core-filling of liquid aluminum and the formation of hollows, shrinkages, or cold shuts in the core (e.g., L = 230 mm).

(2) With the casting temperature of aluminum increasing, the SLI position of aluminum moves along the withdrawal direction, and the reasonable range of casting temperature of aluminum is 1003-1083 K.

(3) With the increase of secondary cooling water flux, the SLI position of aluminum moves against the withdrawal direction and the reasonable range of secondary cooling water flux is 600-900 L·h^{-1}.

(4) The mean withdrawing speed has a significant influence on the temperature field of HCFC process. Increasing the mean withdrawing speed results in the SLI shifting of copper and aluminum along the withdrawal direction and the increase of interface temperature during HCFC for CCA rods. In this study, the reasonable range of mean withdrawing speed is 75-80 mm·min^{-1}, and the casting process for CCA rods is continuous and stable.

Acknowledgements

This work was financially supported by the National High Technology Research and Development Program of China (No. 2013AA030706 and No. 2009AA03Z532) and the Fundamental Research Funds for the Central Universities of China (No. FRF-TP-12-146A). The authors thank Yu Lei and Jun Mei for their help with the experiments, and Prof. Zhi-Hao Zhang and Dr. Yan-Bin Jiang for helpful discussion.

References

[1] A. Gibson, Emerging applications for copper-clad steel and aluminum wire, *Wire J. Int.*, 41(2008), No. 2, p. 142.

[2] K. Nakasuji, K. Masuda, and C. Hayashi. Development of manufacturing process of clad bar by rotary rolling, *ISIJ Int.*, 37(1997), No. 9, p. 899.

[3] T. Yamaguchi, T. Takayama, and M. Hiderita, *Method for Producing Copper Clad Aluminum Wire*, USA Patent, Appl. 3854193, 1974.

[4] K.Y. Rhee, W.Y. Han, H.J. Park, and S.S. Kim, Fabrication of aluminum/copper clad composite using hot hydrostatic extrusion process and its material characteristics, *Mater. Sci. Eng. A*, 384(2004), No. 1-2, p. 70.

[5] N. F. Neumann, *Continuous Casting*, USA patent, Appl. 3421569, 1969.

[6] J.X. Xie, C.J. Wu, X.F. Liu, and X.H. Liu, A novel forming process of copper cladding aluminum composite materials with core-filling continuous casting, *Mater. Sci. Forum*, 539-543(2007), No. 1, p. 956.

[7] Y.J. Su, X.H. Liu, H.Y. Huang, C.J. Wu, X.F. Liu, and J.X. Xie, Effects of processing parameters on the fabrication of copper cladding aluminum rods by horizontal core-filling continuous casting, *Metall. Mater. Trans. B*, 42(2011), No. 1, p. 104.

[8] Y.J. Su, X.H. Liu, H.Y. Huang, X.F. Liu, and J.X. Xie, Interfacial microstructure and bonding strength of copper cladding aluminum rods fabricated by horizontal core-filling continuous casting, *Metall. Mater. Trans. A*, 42(2011), No. 13, p. 4088.

[9] A. Ramírez-López, R. Aguilar-López, M. Palomar-Pardavé, M.A. Romero-Romo, and D. Muñoz-Negrón, Simulation of the heat transfer on steel billets during continuous casting, *Int. J. Miner. Metall. Mater.*, 17(2010), No. 4, p. 403.

[10] Y.J. Xia, F.M. Wang, J.L. Wang, and G.Z. Li, Simulation

of the continuous casting process in a mold of free-cutting steel 38MnVS based on a MiLE method, *Int. J. Miner. Metall. Mater.*, 18(2011), No. 5, p. 562.

[11] A.K. Tieu and I. S. Kim, Simulation of the continuous casting process by a mathematical model, *Int. J. Mech. Sci.*, 39(1997), No. 2, p. 185.

[12] A.F. Mills, *Heat Transfer,* 9th Ed., Prentice Hall Inc, Upper Saddle River, 1999, p. 147.

[13] J.R. Davis, *Copper and copper Alloys*, ASM International, Materials Park, 2001, p. 446.

[14] F. King, *Aluminium and Its Alloys*, Halsted Press, New York, 1987, p. 22.

[15] S.H. Li, *Products of Carbon and Graphite*, Metallurgical Industry Press, Beijing, 1983, p. 32.

[16] J.R. Welty, *Engineering Heat Transfer*, John Wiley & Sons, Inc., New York, 1978, p. 213.

[17] D.C. Weckman and P. Niessen, A numerical simulation of the D.C. continuous casting process including nucleate boiling heat transfer, *Metall. Trans. B*, 13(1982), No. 4, p. 593.

[18] W.M. Rohsenow and J. P. Hartnett, *Handbook of Heat Transfer*, McGraw-Hill Book Company, New York, 1973, p. 13-45.

[19] I.L. Pioro, Experimental evaluation of constants for the Rohsenow pool boiling correlation, *Int. J. Heat Mass Transfer*, 42(1998), No. 11, p. 2003.